Chapter

On-Site Bridge Inspection by 950 keV/3.95 MeV Portable X-Band Linac X-Ray Sources

Mitsuru Uesaka, Yuki Mitsuya, Katsuhiro Dobashi, Joichi Kusano, Eiji Yoshida, Yoshinobu Oshima and Masahiro Ishida

Abstract

Many bridges around the world face aging problems and degradation of structural strength. Visual and hammering sound inspections are under way, but the status of inner reinforced iron rods and prestressed concrete (PC) wires has not yet been confirmed. Establishing a diagnosis method for bridges based on X-ray visualization is required to evaluate the health of bridges accurately and to help with the rationalization of bridge maintenance. We developed 950 keV/3.95 MeV X-band electron linac-based X-ray sources for on-site bridge inspection and visualized the inner structure of a lower floor slab. The information regarding wire conditions by X-ray results was used for the structural analysis of a bridge to evaluate its residual strength and sustainability. For more precise inspection of wire conditions, we applied three-dimensional image reconstruction methods for bridge mock-up samples. Partial-angle computed tomography (CT) and tomosynthesis provided cross-sectional images of the samples at 1 mm resolutions. Image processing techniques such as the curvelet transform were applied to evaluate diameter of PC wires by suppressing noise. Technical guidelines of bridge maintenance using the 950 keV/3.95 MeV X-ray sources are proposed. We plan to offer our technique and guidelines for safer and more reliable maintenance of bridges around the world.

Keywords: bridge inspection, X-ray, nondestructive test, linear accelerator, structural analysis, computed tomography, tomosynthesis, curvelet transform, technical maintenance guidelines

1. Introduction

Maintaining the health of civil infrastructures such as bridges, roads, and tunnels is important to achieve a safe and reliable society [1–3]. Because a large number of concrete structures were built in the age of rapid economic growth in Japan, many of them are approaching their designed life spans. Thus, the development of a reliable health diagnosis technology is currently an urgent task. For example, many of the prestressed concrete (PC) bridges have life spans of 50 years, and they show apparent damage as they approach their designed life spans (**Figure 1**). Approximately 42 and 63% of all bridges will be over 50 years of age by 2021 and 2031, respectively.

(i)

(ii)

(iii)

Figure 1.
Images of degraded bridge and parts. (i) Whole view of the bridge, (ii) degraded surface, and (iii) crack and leak of Ca components.

Normally, concrete bridges are regularly inspected by visual check and hammering tests. If damages or abnormalities are detected, more detailed nondestructive tests (NDTs) must be conducted.

NDT by X-ray radiography is one of the promising technologies for the detailed local inspection of a bridge. X-ray radiography provides high-resolution images of steel wires and rods inside thick concrete bridges. Its penetration capability depends on the thickness of the object and the energy of the X-ray; higher energy X-rays penetrate thicker concrete structures. However, the energy produced by X-ray sources for industrial NDTs is not sufficiently high for the inspection of bridges, because of their thick concrete structure. A low energy source does not provide clear contrast inside the concrete, and in addition, the exposure time required is very long. Some radioisotopes provide high-energy X(γ)-rays. However, they continuously emit X(γ)-rays and operator health becomes another concern. Thus, a new, safer bridge inspection technology using high-energy powerful X-ray sources is needed.

We have developed X-band electron linear accelerator (linac)-based portable X-ray sources with high maximum energies of 950 keV and 3.95 MeV and have been demonstrating X-ray inspection of infrastructures using these sources [4–7]. We have successfully conducted ten on-site inspections using these X-ray sources to date, and we are also working on technology development in laboratories using samples from dismantled bridges.

The main focus of X-ray visualization of a bridge is damage of prestressed concrete (PC) wires and unfilled sheath pipes. Not only the rupture of wires but also the wastage of wires by corrosion reduces the residual strength of a bridge. Therefore, the quantitative evaluation of wire diameters within a resolution of 1 mm is required for X-ray imaging. The grout fill in the sheath pipes of a PC bridge is important to prevent wire corrosion from rainwater and to make the wires and the concrete operate as a composite material. Detecting unfilled sheath pipe areas by X-ray is therefore important for detecting wire damage or for calculating stress imbalances in the bridge. The results of X-ray visualization are used to evaluate the residual strength of a bridge using a reliable numerical calculation method.

The goal of our research is to establish a structural health diagnosis method based on X-ray imaging of the inner structure of a bridge. In this chapter, we present the results of X-ray imaging of an actual bridge still in use and the calculated results of its residual strength through a numerical simulation. Investigation of the validity of X-ray partial-angle computed tomography (CT) or tomosynthesis image reconstruction for precise bridge inspection was also performed.

2. X-ray inspection and structural analysis of a bridge

2.1 950 keV/3.95 MeV X-ray sources

We used X-band (9.3 GHz) linac-based 950 keV/3.95 MeV X-ray sources for the inspection of the actual bridge. The systems are shown in **Figures 2** and **3**, respectively.

In the former, the electrons are accelerated up to 950 keV by radio-frequency (RF) fields. We also adopted the side-coupled standing wave-type accelerating structure. Electrons are injected into a Tungsten target that generates bremsstrahlung X-rays. The generated X-rays are collimated by a Tungsten collimator into the shape of a cone which has an opening angle of 17°. The most important is the X-ray intensity, which is 50 mSv/min at 1 m for a full magnetron RF power of 250 kW. The system consists of a 50-kg X-ray head, 50-kg magnetron box, and stationary electric power source and water chiller unit. The X-ray head and magnetron box are portable, and because they are connected to each other by a flexible waveguide, only the position and angle of the X-ray head are finely tuned. We have optimized the design with respect to X-ray intensity, compactness, and weight. The

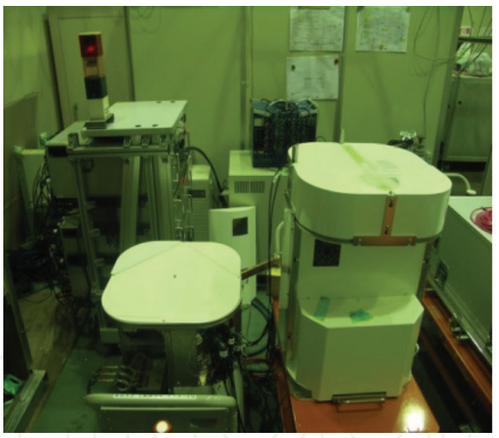

Operating frequency	9300 MHz
Beam energy	950 keV
Beam current	130 mA
Pulse width	2.5 μs
Pulse frequency	330 pulses/s
RF power	250 kW
Electron gun voltage	20 kV
Accelerator length	125 mm
Q-value of the accelerator	7150
X-ray size at target	0.7 mm
X-ray intensity at 1 m	> 50 mGy min^{-1}

Figure 2.
950 keV portable X-band linac-based X-ray source and its specifications. The maximum X-ray energy is 950 keV. The system consists of three units: X-ray head, magnetron, and power units.

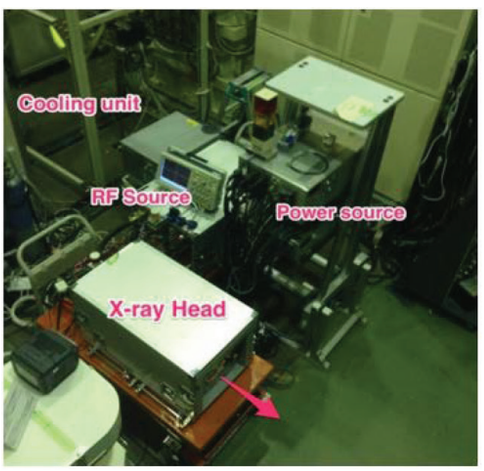

Main unit	Accelerating tube	RF Source	HVPS Control
Weight (kg)	80+62 (Collimator + Accelerating tube)	62	116
Parameters	Electron gun output current 300mA	Frequency 9.3GHz	
	Electron gun voltage 20kV	Pulse width 4μs	
	Beam current 100mA	Repetition rate 200pps	
		RF power output 1.5 MW	

Figure 3.
3.95 MeV portable X-band linac-based X-ray source and its major parameters. The system consists of four units: X-ray head, magnetron, power, and chiller units.

parameters of the 950 keV X-ray source are summarized in the table of **Figure 2**. We place an X-ray detector on the opposite site of the X-ray source between the object and source to detect the transmitted X-rays through the object. We use a flat panel detector (FPD) from PerkinElmer Corporation for the detector.

The 3.95 MeV system is shown in **Figure 3**. This system consists of a 62-kg X-ray head with target collimator of 80 kg, magnetron box of 62 kg, electric power sources of 116 kg, and water cooling system of 30 kg. The X-ray head and magnetron box are portable, and the position and angle of the former are also finely tuned. The X-ray intensity of this system is 2 Gy/min at 1 m.

Calculated attenuations in concrete for the X-rays from the 950 keV/3.95 MeV sources are shown in **Figure 4**. The results indicate that concrete with thicknesses of up to 400 mm and 800 mm can be penetrated by the 950 keV/3.95 MeV sources, respectively.

2.2 Compliance

We comply with Japan's Law Concerning Prevention of Radiation Hazards Due to Radioisotopes and Regulations on Prevention of Ionizing Radiation Hazards when we use the 950 keV/3.95 MeV X-ray sources in the field for on-site bridge inspection. According to the law, an electron beam source below 1 MeV is not

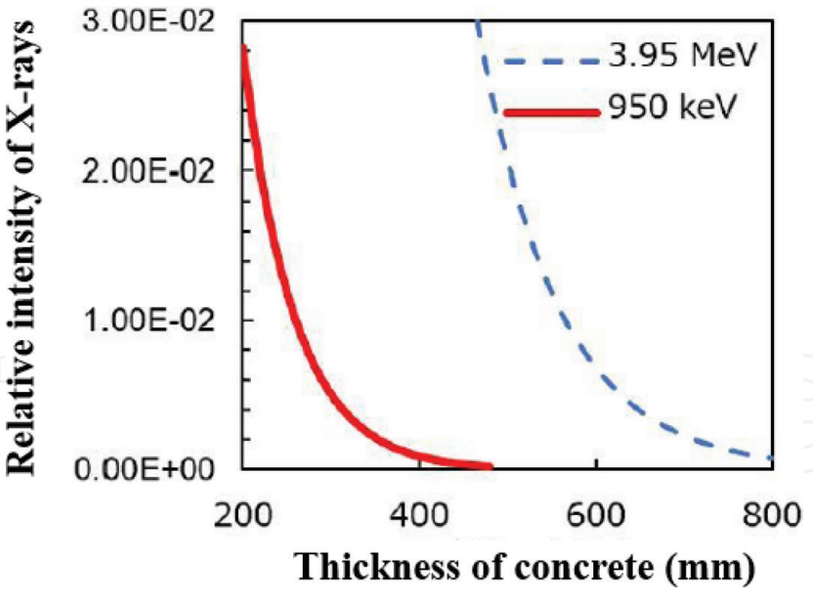

Figure 4.
Calculated results of attenuation for the X-rays in concrete from the 950 keV/3.95 MeV X-ray sources.

an accelerator. Thus, we comply with this regulation. The 950 keV X-ray source is registered with the local agency of labor supervision. We usually operate the source in a radiation-controlled area, which has a radiation safety system complying with the Regulations on Prevention of Ionizing Radiation Hazards. The use of the source outside the controlled area is also allowed. In this case, we temporally set up a controlled area at the measurement site and place sufficient shielding around the source and object to suppress the air dose rate below 1.3 mSv/3 months. Moreover, we have to set a temporal facility boundary of 250 μSv/3 months. Amendment of the law that allows the use of accelerators below 4 MeV only for on-site bridge inspection was implemented in Japan in 2005. After we completed governmental registration as a radiation source, we submitted for permission of use outside the radiation-controlled area. Finally, we performed the on-site inspection under the Regulations on Prevention of Ionizing Radiation Hazards similar to the 950 keV case.

2.3 X-ray transmission imaging

Three types of PC bridges (T-shaped bar type, box-shaped type, and hollow floor bar type) are investigated by the X-ray sources. Possible patterns of X-ray transmission and scanning (partial-angle CT and tomosynthesis) are depicted in **Figure 5**. An X-ray flat panel detector (FPD) and imaging plate (IP) are used for X-ray imaging acquisition. By using the FPD, online measurement in seconds is available so that sparse and fine-tuning of the position of the X-ray sources and detector can be accomplished. Stacking measurement in minutes is more appropriate for the IP. Imaging processing of IPs can be carried out on-site immediately. An aerial work platform and stage are used for measurement of the web and flange parts of a T-shaped bar bridge. The X-ray source can be installed inside a box for bottom floor slab inspection or on a pedestal for upper slabs of box-shaped bar types with the help of a crane. As for hollow floor bar types, the X-ray source is placed on the road or inside a hollow box. Even partial-angle CT and tomosynthesis are applicable for those types of inspections.

Figure 6 shows typical transmission images of the inner structure of the slab of a certain T-shaped bar-type bridge obtained by the 950 keV X-ray source. We successfully observed the inner structure in detail with the linac-based X-ray system.

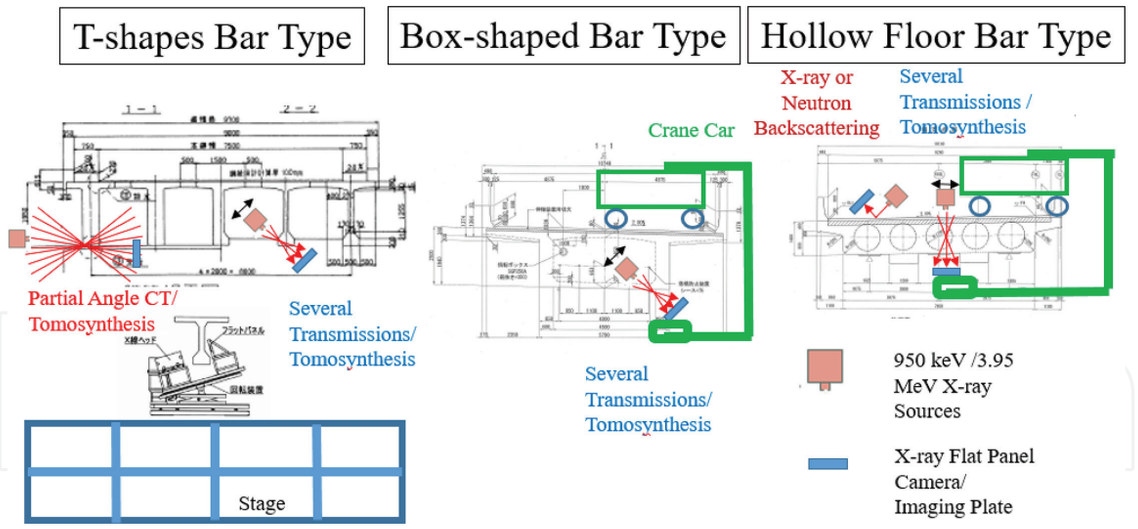

Figure 5.
Typical techniques of X-ray transmission/scanning inspections for bridges of T-shaped bar type, box-shaped bar type, and hollow floor bar type.

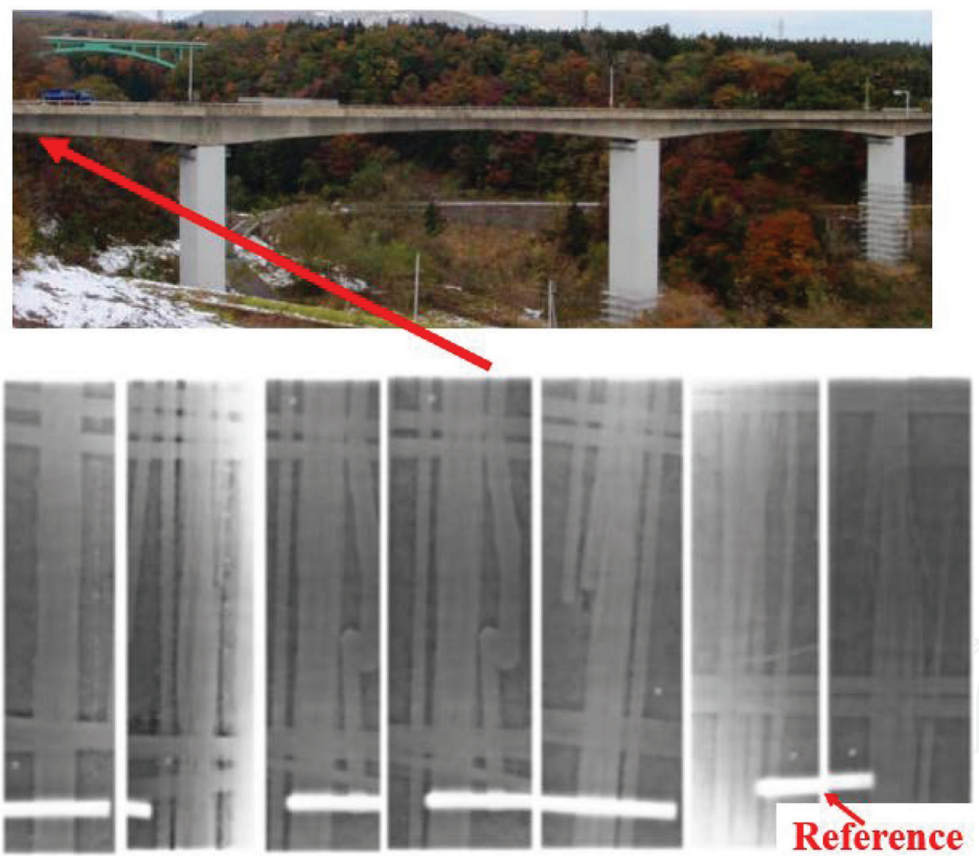

Figure 6.
Series of X-ray images of PC wires in a bottom slab of a box-shaped bar-type bridge acquired by the 950 keV X-ray source. Cutting and thinning of PC wires are observed.

The PC wires were clearly visualized. Cutting and thinning of PC wires are clearly apparent. Reduction of the PC wire cross sections is estimated visually, and images are used for the structural analysis to evaluate any reduction of structural strength quantitatively.

PC wires, sheath, and grout in a web part of other T-shaped bar types obtained by the 950 keV X-ray source are given in **Figure 7**. Even grout filling and missing grout are clearly visible.

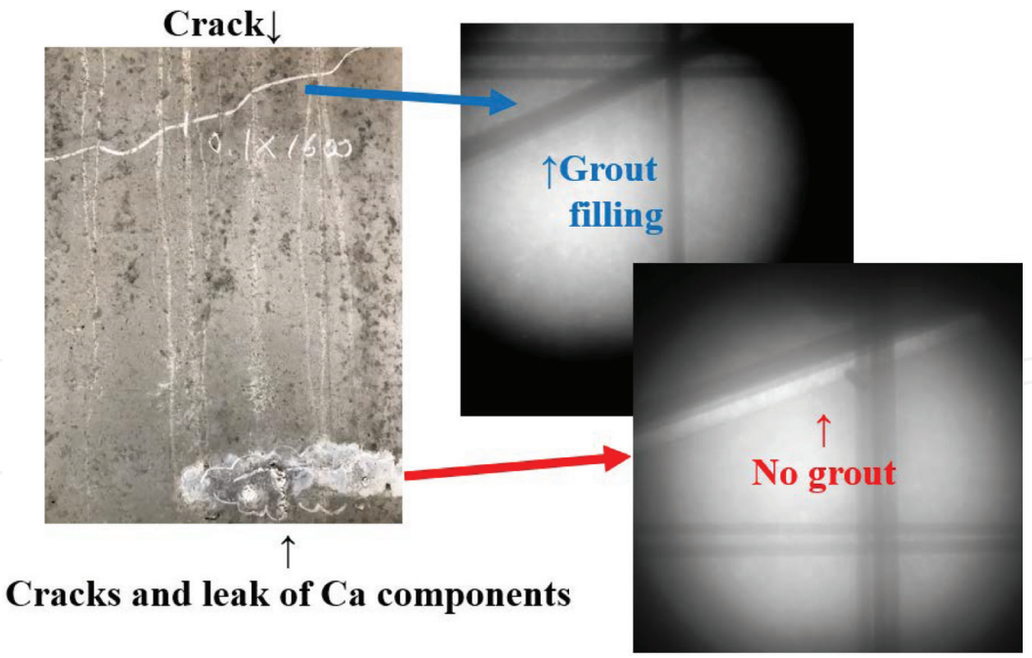

Figure 7.
Surface view and X-ray transmission images of near PC wires, sheath, and grout in a web part of a T-shaped bar-type bridge acquired by the 950 keV X-ray source. Cracks and leak of Ca components are visible. Moreover, grout filling and missing grout are clearly observed in the near PC sheath.

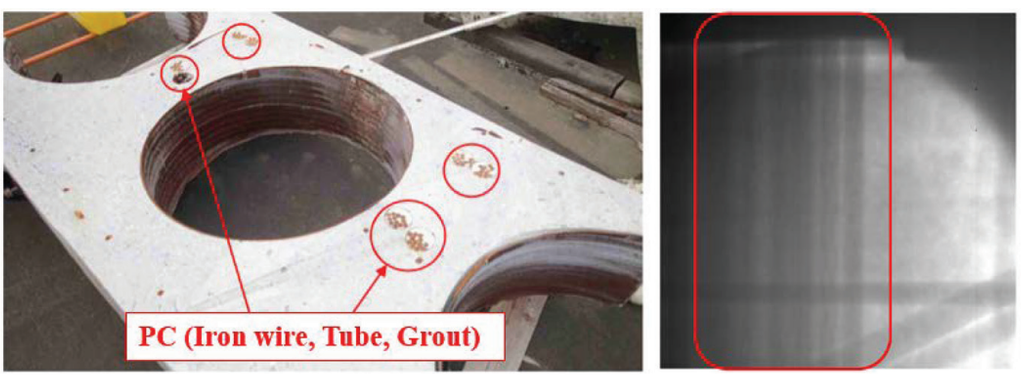

Figure 8.
Cut sample from a hollow flow bar-type bridge and X-ray transmission image acquired by the 3.95 MeV X-ray source. The total thickness of the concrete where the X-rays penetrate is ~400 mm. Several PC wires located deep in concrete are visualized.

Figure 8 shows an X-ray transmission imaged by the 3.95 MeV X-ray source from a cut sample of a hollow flow bar-type PC bridge. Several PC wires located deep in the concrete are visualized.

However, the contrast between the wires and concrete was not sufficiently high. We consider that one reason is noise produced by X-rays scattered by the concrete structure. The probability of Compton scattering of an X-ray becomes higher as the energy of the X-ray becomes higher. If Compton scattering occurs between an X-ray photon and an atom of the material, the photon loses a portion of its energy and changes its direction. Because the original energies of X-rays are high, the energies of scattered X-rays are also high. Thus, many photons may have been scattered within the concrete structure and were detected at the FPD. It is an important task to reduce the image noise caused by scattering X-rays. A possible means to resolve this issue is by introducing a fine pitch metal mesh in front of the FPD to absorb only the X-rays impinging on the FPD and block scattered X-rays coming from other directions. Of course, image processing can be used to reduce noise. This aspect is discussed later.

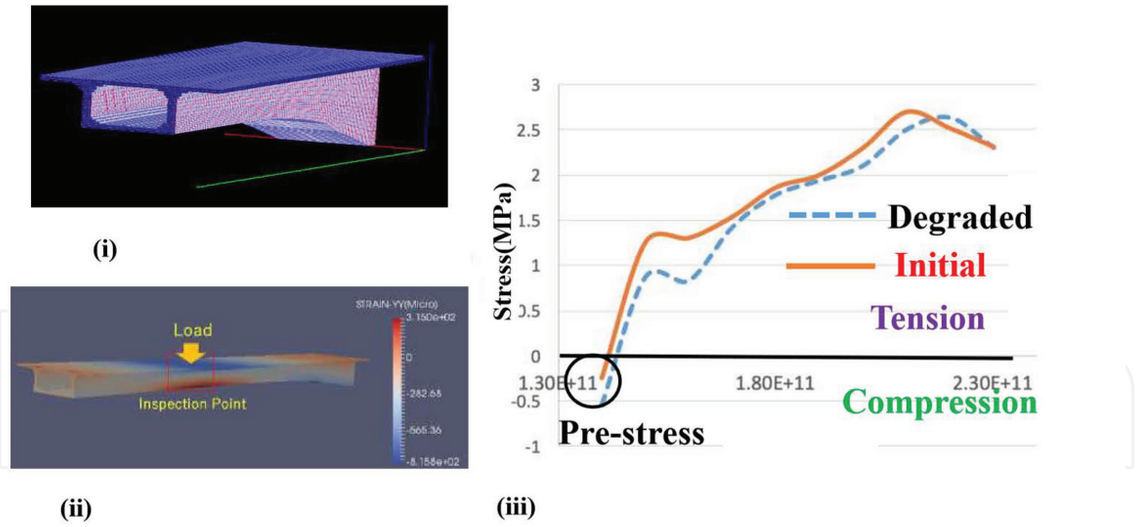

Figure 9.
Typical results of 3D nonlinear structural analysis of iron-reinforced concrete based on DuCOM-COM3 simulation using the cross-sectional reduction based on the measured X-ray transmission images such as those in **Figure 6**. *Mesh model of the finite element method (FEM) and typical load pattern for structural degradation evaluation and stress contour results are shown in (i) and (ii), respectively. Curves of applied moment versus stress for the initial and degraded (measured) states are shown in (iii).*

2.4 Three-dimensional structural analysis

We calculated the residual strength of a block of the bridge using X-ray inspection results and the 3D nonlinear three-dimensional finite element method (FEM) software for reinforced concrete, named DuCOM-COM3 developed by Prof. Hirokazu Maekawa (Department of Civil Engineering, University of Tokyo). The model for FEM analysis is shown in **Figure 9**. We modeled a block of the bridge with an X-ray inspected part at its center, as shown in **Figure 9(i)**. The X-ray inspected part is 1600 mm in the longitudinal direction. The boundary conditions were the moments when the designed load is applied, which were calculated by Newmark's method.

As a result of the FEM analysis, we found that the stress increased about 0.3 MPa at the lower edge of the box girder. This is because the stress resistance was decreased owing to damage of some PC wires. On the other hand, the compressive stress at the upper edge was not affected. The 3D distributions of stress after wire damage are depicted in **Figure 9(ii)**. From the calculations, the load that generates concrete cracks is estimated as 8417 kN for the healthy condition and 8016 kN for the damaged condition. Curves of given moment versus stress for the initial and degraded states are shown in **Figure 9(iii)**. Although the residual strength decreased by approximately 5%, the stress after damage remained within the range of the allowable stress, and the bridge was judged as operable at its current condition.

3. Three-dimensional image reconstruction methods for bridge inspection

3.1 Computed tomography and tomosynthesis for partial angle

Three-dimensional information of the inner structure of the concrete bridge is more helpful than a simple X-ray transmission image if the structure is complicated by densely concentrated wires. In a simple radiography image, the wires are superimposed, and thus a precise evaluation of wire condition is not possible. However,

in a three-dimensional image, each wire can be separated, and evaluating the diameters of the wires is easier and more precise.

X-ray CT has been a powerful tool used for this type of purpose in a wide variety of fields, such as medical and industrial applications. In a CT system, the X-ray source and the detector are rotated 360° around the object, and X-ray images are obtained at different angles. Slice images of the object will be reconstructed from the X-ray absorption factors calculated from the images. CT is widely used for the precise inspection of industrial products in the field of NDT; thus, we can expect it is also applicable for bridge inspections using higher energy X-rays.

However, it is usually impossible to widely rotate the source and detector around a target part of a bridge because of limited spaces around the target. We therefore consider applying partial-angle CT for bridge inspections. In partial-angle CT, the source and the detector are rotated less than 360°, and cross-sectional images are reconstructed from those partial-angle projection images. Partial-angle CT formulation is explained as follows, and its coordinate system for the spatial domain is illustrated in **Figure 10(i)**. When the 2D X-ray attenuation constant distribution is $f(x, y)$, the relation between the initial X-ray intensity from the X-ray source, I_0, and input intensity at the detector, I_i, along the arrow in the figure is approximately given as

$$I_0 = I_i \exp\left\{-\int_s f(x,y)ds\right\}, \tag{1}$$

$$\int_s f(x,y)ds = \ln\frac{I_i}{I_0}. \tag{2}$$

Therefore, the Radon integral is measured by

$$p(r,\theta) = \int_{-\infty}^{\infty} f(x,y)ds = \int_{-\infty}^{\infty}\int_{-\infty}^{\infty} f(x,y)\delta(x\cos\theta + y\sin\theta - r)dxdy. \tag{3}$$

The Fourier transform of $f(x, y)$, $F(\mu, v)$, is given by the measured Radon transform data as

$$\begin{aligned} F(\mu,v) &= \int_{-\infty}^{\infty}\int_{-\infty}^{\infty} f(x,y)\exp\{-j2\pi(\mu x + vy)\}dxdy \\ &= \int_{-\infty}^{\infty} p(r,\theta)\exp(-j2\pi\rho r)dr, \end{aligned} \tag{4}$$

where

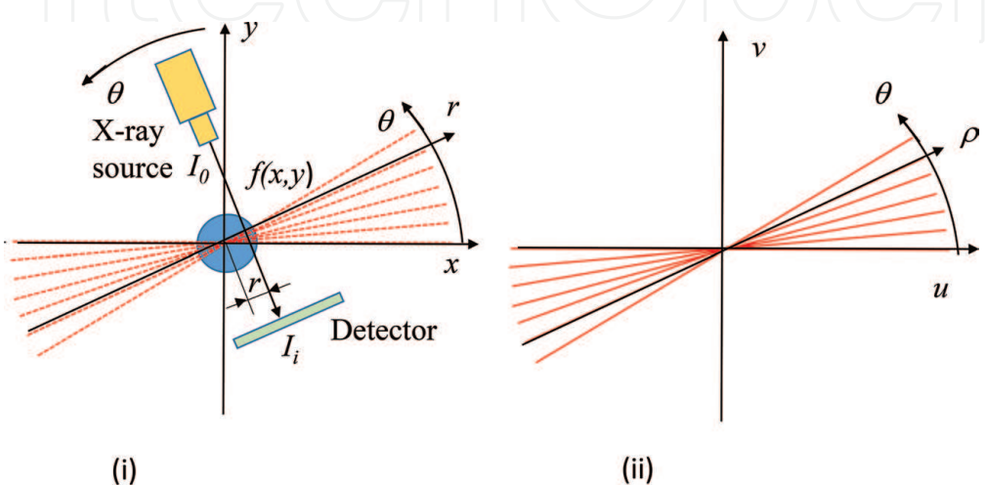

Figure 10.
Coordinate system for the partial-angle CT. (i) Spatial domain, and (ii) Frequency domain.

$$\mu = \rho\cos\theta, v = \rho\sin\theta,$$

$$\rho = \sqrt{u^2 + v^2},$$

and the coordinate system in the frequency domain is shown in **Figure 10(ii)**. In case of the partial-angle CT, the angle range is rather limited so that the Fourier transform data cannot be obtained in the whole frequency domain. Finally, the original X-ray attenuation distribution is calculated numerical by the filtered back projection method in the following:

$$f(x,y) = \int_{-\infty}^{\infty}\int_{-\infty}^{\infty} F(\mu,v)\exp\{j2\pi(\mu x + vy)\}d\mu dv. \quad (5)$$

Typical results for limited angles are introduced in Section 3.2.

Another promising technology for obtaining three-dimensional information inside a bridge is tomosynthesis. Tomosynthesis has been used for applications such as breast imaging or dental imaging [8]. In normal tomosynthesis, the source is rotated against the detector with limited angle, and "parallax" X-ray images are obtained. The cross-sectional images of a target object are reconstructed from the parallax images. Tomosynthesis has been used in applications where full-angle CT cannot be applied. Thus, it is also a promising technology for bridge inspections.

As a first step, we experimentally investigated the feasibility of partial-angle CT and tomosynthesis using mock-up samples of bridges.

3.2 Image reconstruction

We have applied the partial-angle CT and tomosynthesis to cut samples from the real PC bridge and acrylic phantoms.

The CT reconstructed results for PC wires in a cut sample of the flange part of a T-shaped bar bridge by scanning at 360, 180, and 90° using the 3.95 MeV X-ray

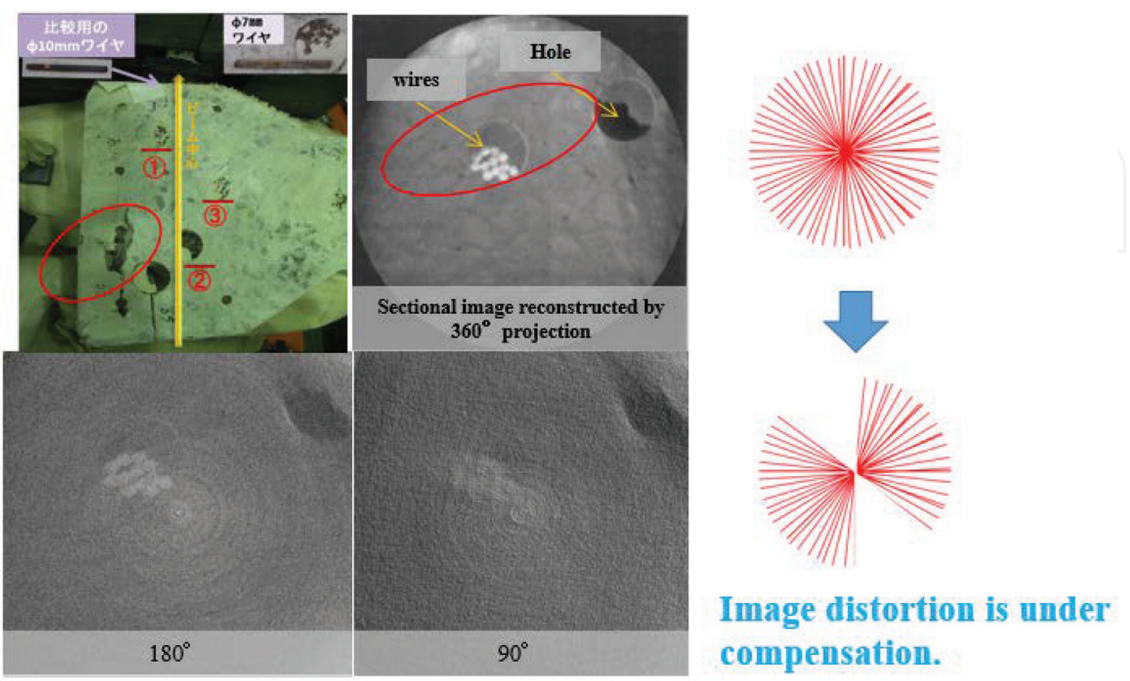

Figure 11.
CT reconstructed results of PC wires in the flange part of a T-shaped bar bridge by scanning at 360, 180 and 90° using the 3.95 MeV X-ray source. All PC wires in a sheath are perfectly reconstructed by 360° scanning.

source are shown in **Figure 11**. All PC wires in a sheath are perfectly reconstructed by 360° scanning. The circular shape is intrinsically deformed to an elliptic shape by partial-angle scanning using the CT algorithm. However, the minor axis diameter of the ellipse is almost the same as the real diameter of the PC wires.

Figure 12 is a reconstructed image of the cross section of an acrylic phantom by tomosynthesis. Although we also observed the deformation of the cross-sectional shapes from circles to ellipses in tomosynthesis, we can estimate the original diameters from the minor axes of the ellipses. We extracted a profile from

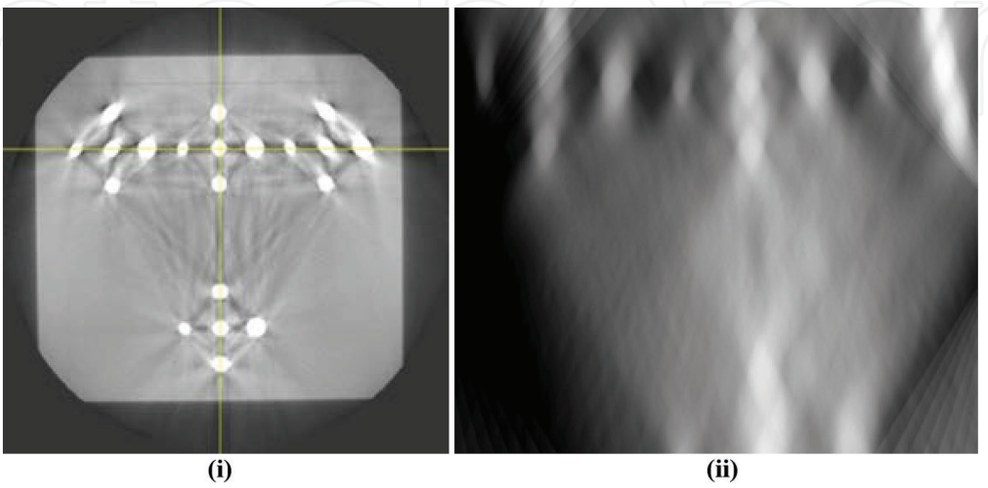

Figure 12.
Cross-sectional X-ray images of the acrylic phantom reconstructed by (i) full-angle CT and (ii) tomosynthesis. The tomosynthesis image was obtained with 25 projections taken in 3° steps.

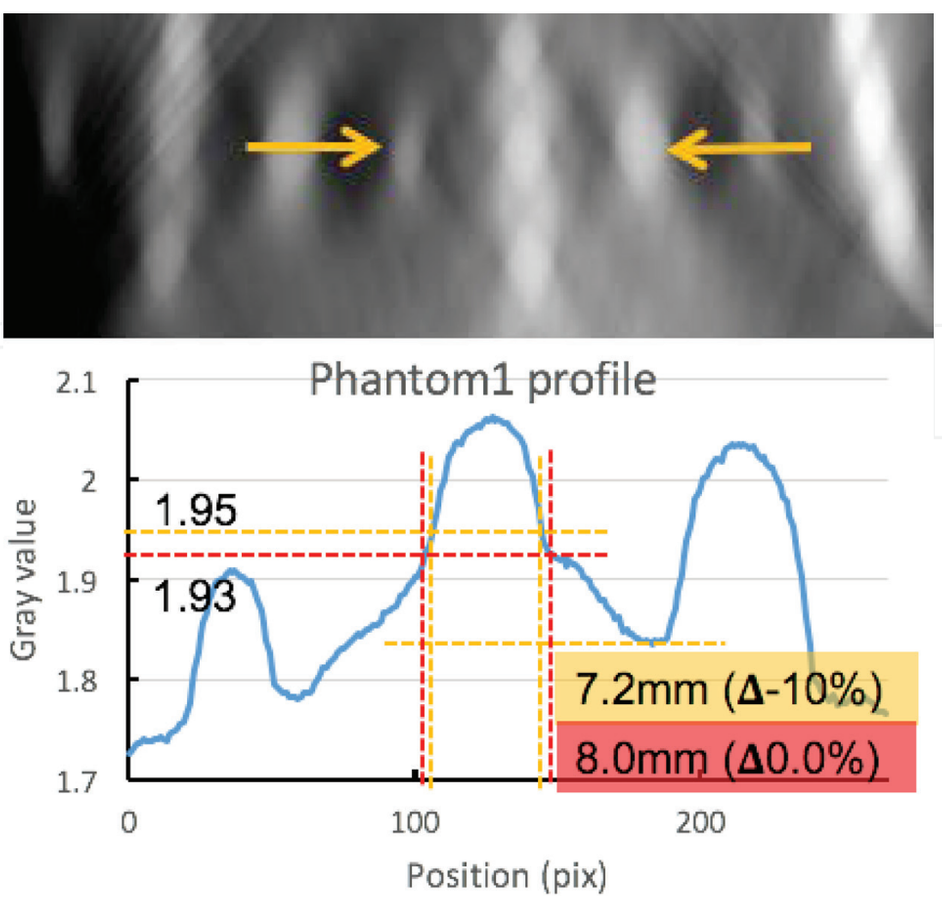

Figure 13.
Gray value plot of a profile in the tomosynthesis image of the acrylic phantom.

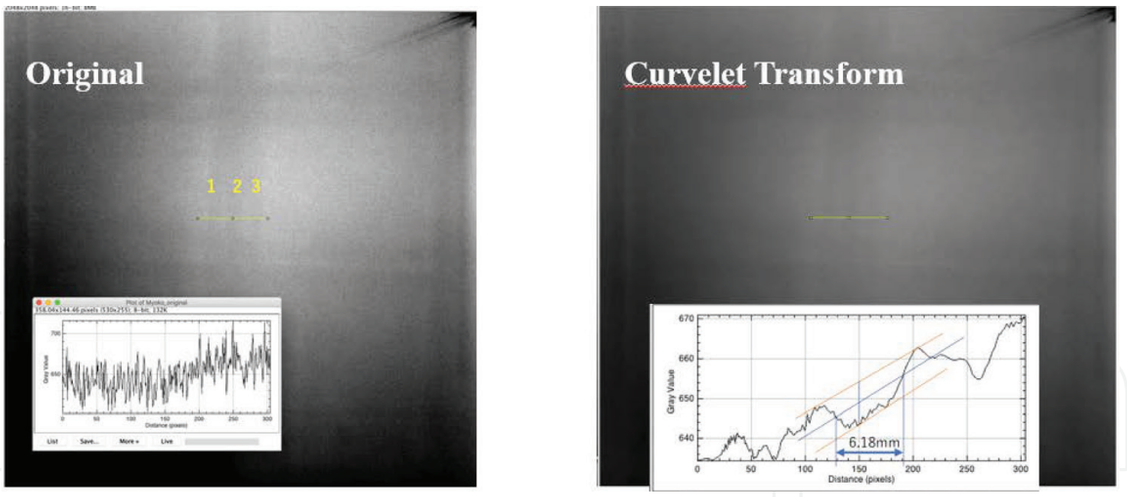

Figure 14.
Image processing using the curvelet transform and evaluation of the diameter of PC wires.

the tomosynthesis image and plotted its gray values (see **Figure 13**). The profile included three rods with different diameters (6, 8, and 10 mm). We were able to estimate the diameter of the center rod (8 mm) within 1 mm accuracy. From the profile plotting, the estimated diameter of the rods was between 7.2 and 8.0 mm.

3.3 Image processing

Software image processing is inevitable for this work. Fourier transform (FT) with low-pass filter, high-pass filter, and band-pass filter is a standard technique. If we apply FT with a low-pass filter, the image becomes blurred, and the boundary between an iron rod and a PC wire is difficult to recognize. As for FT with a high-pass filter, the boundary is emphasized, but the overall view is spotty. When we construct a gray value profile to evaluate the diameter of a rod or PC wire, the profile is noisy. Regarding a band-pass filter, trial and error is necessary to choose an appropriate band. Instead, the wavelet transform is effective for emphasizing local signals. Recently, the curvelet transform has become popular. It is an upgraded wavelet transform fit to emphasize curved and declined boundaries. We applied the curvelet transform to the X-ray transmission images of PC wires of the upper slab of the hollow box bar-type bridge (**Figure 6**). We attempted to evaluate the diameter of one of the PC wires in the somewhat blurred image of the 400 mm slab, which is close to the transmission limit of the X-rays from the 950 keV source. We can observe that spatially high-frequency noises are suppressed and the full width at half maximum (FWHM) can be used to estimate the diameter, which is 6.18 mm for the designed 7 mm wire as shown in **Figure 14**.

4. Highlights from recent inspections of real bridges

4.1 Relationships between states of concrete surface and near PC wires

We check the relationship between the states of a concrete surface and near inner PC wires. We evaluate cut samples from a decommissioned T-shaped bar-type bridge. One example is shown in **Figure 15**. The surface concrete is somewhat degraded and cracked (see **Figure 15(i)**). The cut cross-sectional view and X-ray transmission image of the near PC wires are shown in **Figure 15(ii)** and **(iii)**, respectively. The PC wires look healthy in this case. Because this bridge was located near the sea, the degradation of the concrete was due to salt damage. Furthermore, a load

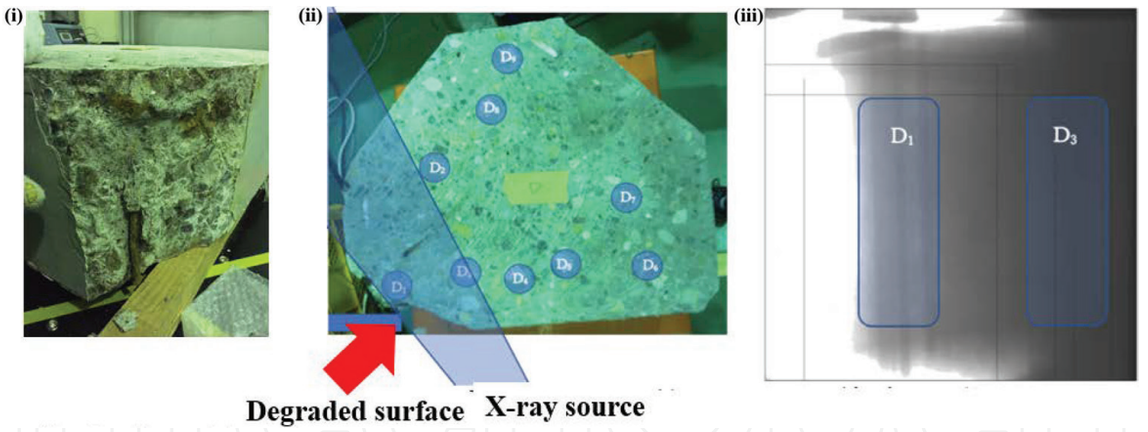

Figure 15.
Typical case of heavily corrupted concrete surface (i) and healthy PC wires in a cut sample from a T-shaped bar bridge. The direction of the X-ray transmission is shown in (ii). X-ray transmission images of PC wires in two sheaths are shown in (iii).

test was performed on this bridge. It was confirmed that its mechanical strength was not degraded, and this mechanically healthy bridge was wastefully decommissioned.

In the above case, inner PC wires were healthy even though the surface concrete was degraded and cracked. Opposite cases involving corroded PC wires in bridges with healthy surface concrete have also been found.

These facts indicate that visible and hammer-sound inspections are not necessarily sufficient for checking the degradation of a bridge's mechanical strength. X-ray inspection is needed to check the state of inner PC wires and to evaluate the mechanical strength of a bridge.

4.2 Filling and missing grout in PC sheath

X-ray transmission images using the 950 keV source in the web part of the T-shaped bar-type bridge in the case of **Figure 7** overlap at the designated location of the two PC sheaths and wires, as shown in **Figure 16**. Grout fills the upper sheath but is missing in the lower. This is the first observation of grout missing after the initial construction. This vacancy may become a puddle of rainwater which would induce corrosion of PC wires in the near future.

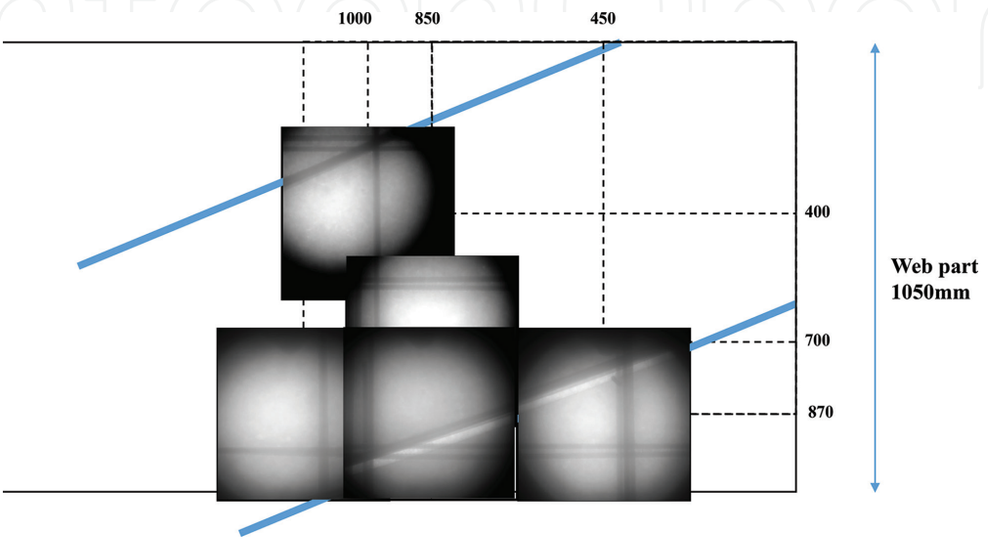

Figure 16.
X-ray transmission images of grout filling and missing grout in the PC sheaths in the web part of a T-shaped bar bridge measured by the 950 keV X-ray source.

Figure 17.
Special inspection car for the 950 keV/3.95 MeV X-ray sources. (i) Front view, (ii) Back view, (iii) Control units, and (iv) On site set-up.

4.3 Special inspection car

Our collaborator, Kanto Giken Co. (Tokai, Ibaraki, Japan), developed a new special inspection car for the X-ray sources as shown in **Figure 17**. It can carry the X-ray sources, detectors, computers, and inspectors and contains a diesel engine 100 V power source. Some diesel engine power sources have poor quality unstable output voltage and frequency (50 and 60 Hz in east and west Japan, respectively). The electric power source of the magnetron may be sensitive to such instability. To avoid this, we decided to acquire our own reliable diesel engine power source, which we can carry to perform on-site X-ray inspections anywhere in Japan.

4.4 Tuning of position and angle of X-ray sources

The most important procedure of this task are the sparse and fine-tuning of the position and angle of the X-ray sources with respect to the bridge part and the X-ray detectors (FPD and IP) as shown in **Figure 18(i)**, **(ii)**, and **(iii)**. The procedure typically requires approximately 1 h. We use an aerial work platform, stage, and special inspection car for initial settings ((i)), and then by using a rotating function of the X-ray head, we adjust its angle. Finally, fine-tuning among the X-ray source, targeted area, and detector is performed. The whole tuning procedure takes approximately 1 h. This procedure consists of using and setting many devices, including the X-ray sources, detectors, mechanical positioners, and so on.

Usually, we start setting up all devices at 9 am. We then perform sparse and fine-tuning of the position and angle of the X-ray sources and detectors and begin taking real measurement at 11 am. We scan several parts until 3 pm. Finally, dismantling and storing the equipment occurs between 3 pm and 5 pm. Targeted bridge parts are

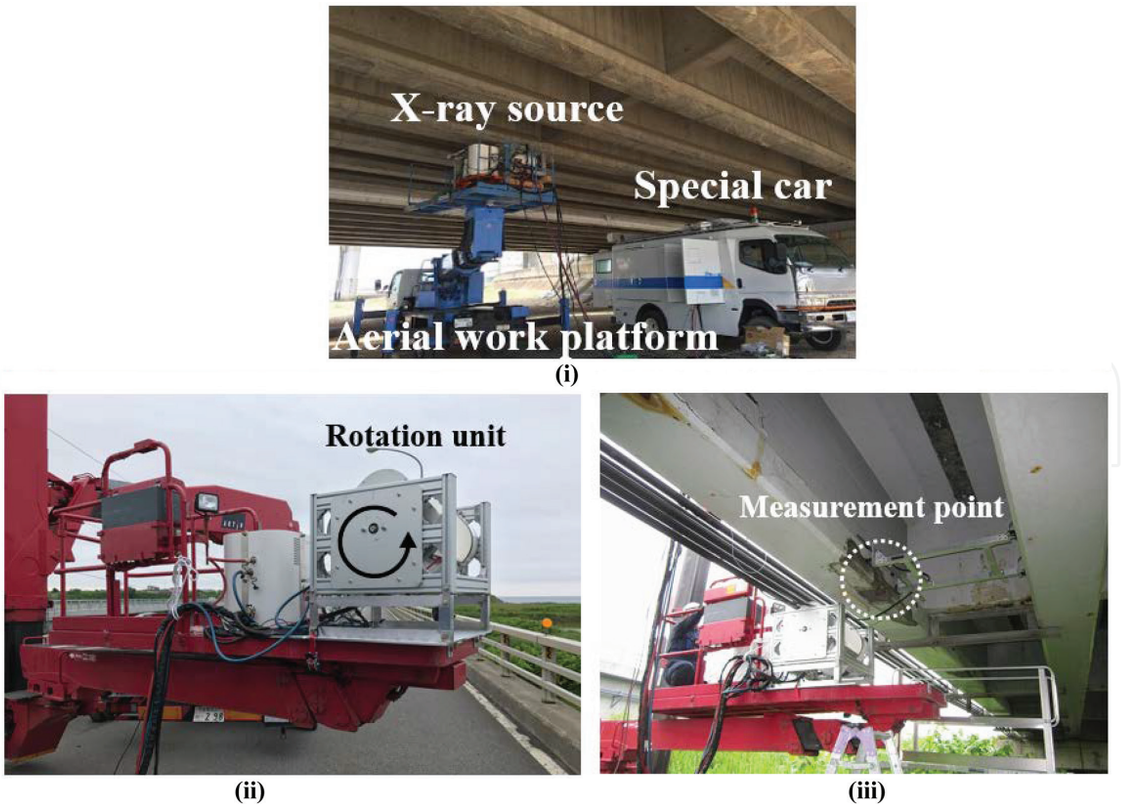

Figure 18.
Initial setup (i), control of angle (ii), and fine positioning (iii) of the 950 keV X-ray source with an aerial work platform.

completely different depending on the three types of bridges (T-shaped bar, box-shaped bar, or hollow floor bar). Thus, we are always improving and upgrading not only the X-ray sources but also our devices and software to better deal with many complicated situations.

Damage to bridges in northern and highland areas in Japan is serious because water in the concrete of a bridge freezes and expands, causing cracks in the concrete. It may snow in those areas in winter. Therefore, inspections should not be carried out during winter. It often rains from June through October in the semitropical climate areas of Japan. We have to be prepared for rain and high humidity, so we use waterproof housing for electric sources and perform very careful equipment treatments and inspections to avoid electric breakdown.

5. Guidelines for special inspections using 950 keV/3.95 MeV X-ray sources

The Public Works Research Institute and the University of Tokyo are developing new technical guidelines for special inspections of bridges using 950 keV/3.95 MeV X-ray sources. An overview is provided in **Figure 19**. First, visual and hammer-sound inspection screening should be performed based on regular inspection guidelines. Advanced hardware and software techniques such as drawn and acoustic analysis are adopted in this step. If degraded parts are found, the special X-ray transmission inspection is performed using the 950 keV or 3.95 MeV X-ray sources, depending on the thickness of the concrete containing the degraded parts. Here, the states of PC wires and rods as affected by corrosion, cuts, and reduction of cross sections are quantitatively evaluated with spatial resolution of 1 mm. Then, 3D nonlinear structural analysis is performed to evaluate

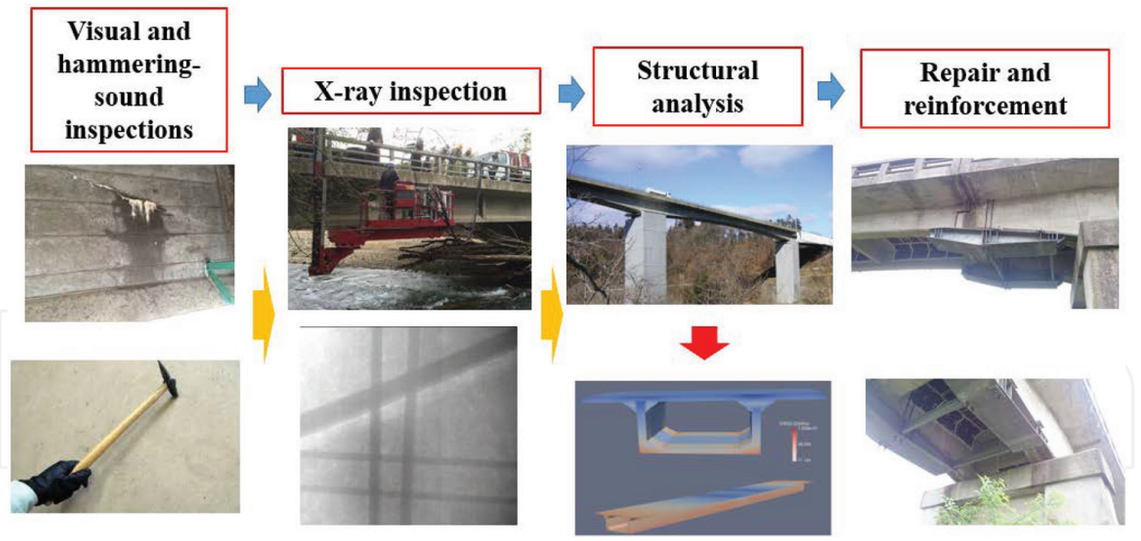

Figure 19.
Guidelines for special X-ray transmission inspection using 950 keV/3.95 MeV X-ray sources accompanied with visual and hammer-sound inspections, structural analysis, final repair, and/or reinforcement.

the degradation of the structural strength quantitatively. Based on this evaluation, repair, reinforcement, or other decisions should be reviewed. Several inspection industries are joining our project and technical transfer is being promoted. We hope to soon apply these guidelines to all aged bridges in Japan and finally across the world.

6. Summary

We have been developing a new X-ray diagnostic method for social and industrial infrastructures using linear accelerator-based X-ray sources. Our 950 keV/3.95 MeV X-ray sources have been applied to many different cases involving on-site X-ray inspection of bridges in Japan. We are currently undertaking on-site inspections of actual bridges. We have demonstrated X-ray inspection of an actual bridge still in use. Clear X-ray transmission images inside the concrete were successfully obtained in the demonstration. The information regarding PC wire conditions from X-ray images was applied to the structural analysis using the finite element method to evaluate the residual strength of a bridge. We found that the residual strength of the bridge in question had decreased by approximately 5% from its original state based on application of the designed load.

We also studied three-dimensional image reconstruction methods that can be applied to bridge inspections. Because of the limitations in spaces and rotation angles involved in actual on-site inspections, full-angle CT is normally not possible to apply for bridge inspections. Thus, we investigated the effectiveness of partial-angle CT and tomosynthesis for bridge inspections. Although the cross-sectional shape of a wire or rod was deformed from its original circular shape to an ellipse-like shape, we could estimate the diameter of the rod or wire from the length of the minor axis of the ellipse. The estimated diameter of a steel rod in a tomosynthesis image was in good agreement with its real value.

Further studies are required to realize the practical use of this X-ray bridge inspection method. We should continue the demonstrations involving on-site bridge inspection for different types of bridges and evaluate the effectiveness of the special X-ray transmission inspection using the 950 keV/3.95 MeV X-ray sources based on the new technical guidelines.

Acknowledgements

This work was supported by the "Infrastructure Maintenance, Renovation, and Management program" of Cross-ministerial Strategic Innovation Promotion Program (SIP), Cabinet Office, Government of Japan. The authors thank for Mr. Kentaro Murata of XIT Co. for the partial CT analysis.

Author details

Mitsuru Uesaka[1*], Yuki Mitsuya[1], Katsuhiro Dobashi[1], Joichi Kusano[2], Eiji Yoshida[3], Yoshinobu Oshima[3] and Masahiro Ishida[3]

1 Nuclear Professional School, School of Engineering, The University of Tokyo, Ibaraki, Japan

2 Accuthera Inc., Kawasaki, Kanagawa, Japan

3 Center for Advanced Engineering Structural Assessment and Research, Public Works Research Institute, Ibaraki, Japan

*Address all correspondence to: uesaka@tokai.t.u-tokyo.ac.jp

References

[1] Chang P et al. Review paper: Health monitoring of civil infrastructure. Structural Health Monitoring. 2003;**2**(3):257-267

[2] Cao H et al. Form-finding analysis of suspension bridges using an explicit iterative approach. Structural Engineering and Mechanics. 2017;**62**(1):85-95

[3] Qin S et al. Dynamic model updating for bridge structures using the kriging model and PSO algorithm ensemble with higher vibration modes. Sensors. 2018;**18**(6):1879

[4] Uesaka M et al. 950 keV, 3.95 MeV and 6 MeV X-band linacs for nondestructive evaluation and medicine. Nuclear Instruments and Methods in Physics Research A. 2011;**657**(1):82-87

[5] Natsui T et al. Development of a portable 950 KeV X-band Linac for NDT. American Institute of Physics Conference Proceedings Series. 2009;**1099**:75-78

[6] Uesaka M et al. Commissioning of portable 950 keV/3.95 MeV X-band linac X-ray source for on-site transmission testing. E-Journal of Advanced Maintenance. 2013;**5**(2):93-100

[7] Uesaka M et al. On-site non-destructive inspection of the actual bridge using the 950 keV X-band electron linac X-ray source. Journal of Disaster Research. 2017;**12**(3):578-584

[8] Niklason LT et al. Digital tomosynthesis in breast imaging. Radiology. 1997;**205**:399-406